Title

Oxidative Uranium Release from Anoxic Sediments under Diffusion-Limited Conditions

Journal

Environmental Science and Technology, 51(19)

ISSN

0013-936X

Authors

Bone, Sharon E

Cahill, Melanie R

Jones, Morris E

et al.

Publication Date

2017-10-03

DOI

10.1021/acs.est.7b02241

Peer reviewed

Oxidative Uranium Release from Anoxic Sediments under Diffusion-Limited Conditions

Sharon E. Bone[*†⊥], **Melanie R. Cahill**[‡], **Morris E. Jones**[‡#], **Scott Fendorf**[‡], **James Davis**[§], **Kenneth H. Williams**[∥], **and John R. Bargar**[†]

[†] Stanford Synchrotron Radiation Lightsource, SLAC National Accelerator Laboratory, Menlo Park, California 94025, United States

[‡] Stanford University, Stanford, California 94305, United States

[§] U.S. Geological Survey, Menlo Park, California 94025, United States

[∥] Lawrence Berkeley National Laboratory, Berkeley, California 94720, United States

DOI: 10.1021/acs.est.7b02241

*Phone: (505) 667-9429; e-mail: shbone@lanl.gov.

Abstract

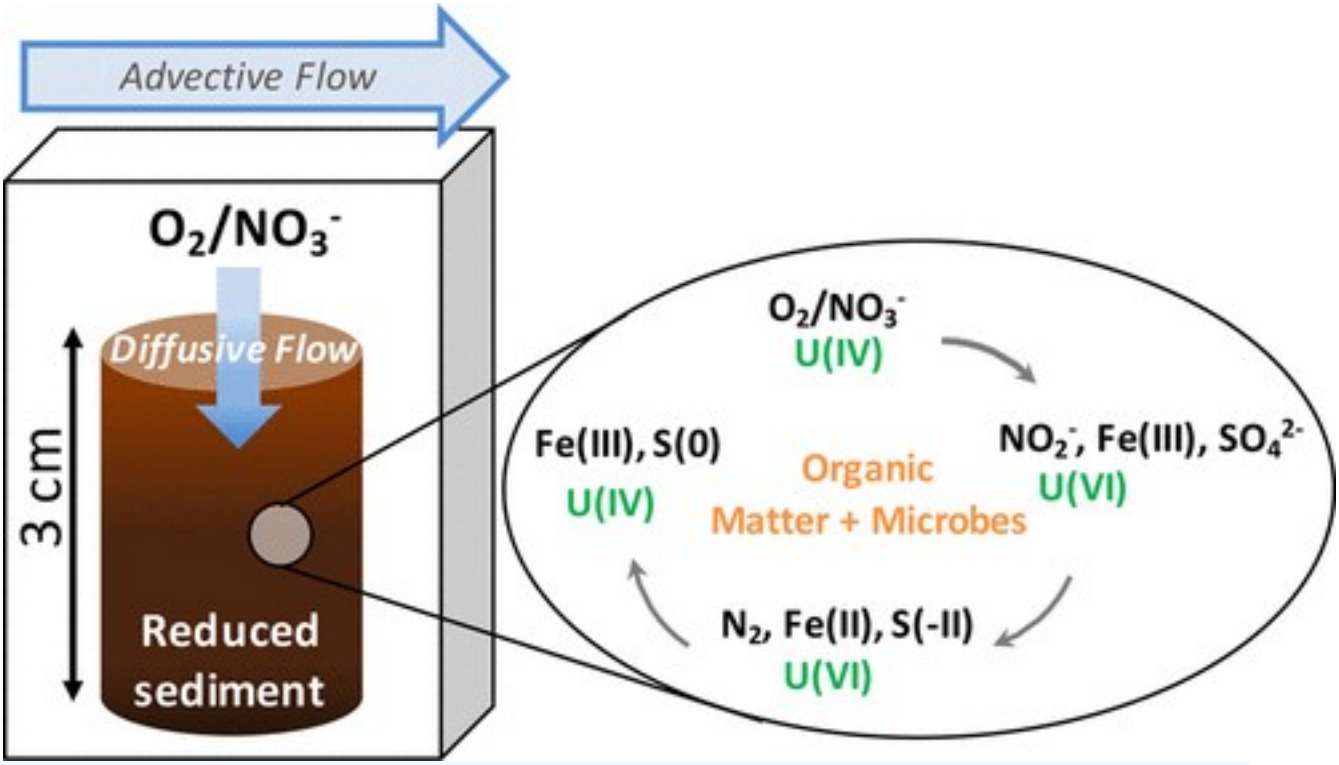

Uranium (U) contamination occurs as a result of mining and ore processing; often in alluvial aquifers that contain organic-rich, reduced sediments that accumulate tetravalent U, U(IV). Uranium(IV) is sparingly soluble, but may be mobilized upon exposure to nitrate (NO_3^-) and oxygen (O_2), which become elevated in groundwater due to seasonal fluctuations in the water table. The extent to which oxidative U mobilization can occur depends upon the transport properties of the sediments, the rate of U(IV) oxidation, and the availability of inorganic reductants and organic electron donors that

consume oxidants. We investigated the processes governing U release upon exposure of reduced sediments to artificial groundwater containing O_2 or NO_3^- under diffusion-limited conditions. Little U was mobilized during the 85-day reaction, despite rapid diffusion of groundwater within the sediments and the presence of nonuraninite U(IV) species. The production of ferrous iron and sulfide in conjunction with rapid oxidant consumption suggested that the sediments harbored large concentrations of bioavailable organic carbon that fueled anaerobic microbial respiration and stabilized U(IV). Our results suggest that seasonal influxes of O_2 and NO_3^- may cause only localized mobilization of U without leading to export of U from the reducing sediments when ample organic carbon is present.

Introduction

Uranium contamination occurs in numerous aquifers throughout the United States and the world as a result of U mining and ore-processing.(1, 2) Where reducing conditions are present, U can be retained in the sediments as U(IV),(3, 4) which is generally less soluble and mobile than U(VI).(5)Elevated groundwater U concentrations exist at many historical ore-processing sites, despite removal of the above ground source material (i.e., mill tailings),(6, 7) suggesting that a mechanism exists within contaminated aquifers to remobilize the U(IV) that has accumulated in the sediments.(8) Fluctuating redox conditions that occur due to seasonal changes in the water table allow introduction of oxidants into sediments as dissolved gases and soluble species,(8, 9) representing a potentially prominent mobilization process. Of particular relevance to fluvial aquifers are the oxidants oxygen (O_2) and nitrate (NO_3^-).(9) The latter can be produced via nitrification when O_2comes into contact with buried organic matter(10) and can be a U cocontaminant due to the use of nitric acid as an extractant.(11) Oxidation of U(IV) by nitrate can occur via bacteria that directly couple it to denitrification,(12) or via direct reaction with denitrification products.(13)

Because U(IV) oxidation can be an important mechanism promoting mobilization and can hinder in situ remediation efforts,(11, 14-16) it has been investigated in numerous laboratory and field studies, yielding information on the processes that may control the rate and extent of oxidation. Such processes include diffusion(17) because U(IV) often

accumulates in fine-grained, low permeability sediments where transport limits the supply of oxidants and induces anoxic conditions.(3, 4, 18) These fine-grained anoxic sediments are distributed as mm to m thick lenses within sand and cobble alluvium.(4) The transport of oxidants is expected to be rapid in the sand and cobble layers where advection predominates, whereas the fine-grained texture of the anoxic sediment could impose diffusion limitations on the availability of oxidants to sedimentary stocks of U(IV). Furthermore, the chemical form of U(IV) has been shown to impact the rate at which U(IV) is oxidized.(19, 20) Finally, other reduced species in anoxic sediments, such as ferrous iron (Fe(II)) and sulfide (S(-II)), which are typically far more abundant than U, could react with oxidants, thereby buffering the oxidation and remobilization of U(IV).(21-23) Among the processes that could influence U(IV) oxidation, the availability of sedimentary organic matter to stimulate microbial consumption of O_2 or NO_3^- has largely been neglected.(24) However, the abundance and microbial availability of organic carbon should be expected to influence the types of microbial respiration that can occur;(25-27) hence the redox poising of the sediments and relative stability of U(IV) and U(VI). This may be particularly important in fluvial aquifers, where buried lenses of organic material accumulate U(IV)(4) and fuel microbial respiration.(10, 28)

Our goal was to investigate U oxidation and release from anoxic sediments under simulated field conditions. We utilized microcosms in which geometrical constraints imposed one-dimensional flow between artificial groundwater and natural, anoxic sediments harvested from a U-contaminated oxbow lake located in Riverton, WY. The artificial groundwater either contained an oxidant (O_2 or NO_3^-) to promote oxidative U release or was free of oxidant to control for other mobilization processes. This design allowed us to assess the importance of different processes that may control the extent to which oxidative U mobilization occurs in the field, including (1) limits on transport imposed by the diffusion-limited flow regime; (2) the speciation of U(IV), hence the rate of U(IV) oxidation; (3) the availability of inorganic reductants that consume oxidant; and, finally, (4) the availability of organic carbon to fuel microbial respiration.

Materials and Methods

Microcosm Design

The sediment used was from the oxbow lake of a former uranium ore-processing site in Riverton, WY.(7) A detailed description of the site, including its geology, legacy of U contamination and remediation strategy is available from Dam et al.(7) Black, fine-grained sediment was collected from the lake bottom and packed into glass jars with metal screw caps. The remaining headspace was filled with water to prevent diffusion of O_2 into the sediment. Sediment was stored at 4 °C before use. The elemental composition of the dried, ground sediment was determined using an X-ray fluorescence analyzer (AMETEK Material Analysis Division, Spectro XEPOS; metals, sulfur and phosphorus content) and an elemental analyzer (Carlo Erba NA1500; carbon and nitrogen content). The U, Fe, C, S and N content of the sediment were 139 ± 5 ppm, 1.7 ± 0.2%, 1.7%, 0.5 ± 0.03%, and 0.08%, respectively. S and Fe K-edge X-ray absorption spectroscopic analysis revealed that sediments were dominated by reduced S species (sulfide, pyrite, and zerovalent sulfur) and that Fe was contained in clay minerals, iron oxides, pyrite, magnetite and some mackinawite, which is consistent with reducing sediments observed in floodplains elsewhere(18)(see Supporting Information, (SI), for details; Figures S1 and S2; Tables S1 and S2).

To replicate the juxtaposition between low-permeability reduced sediment and high-permeability sand and cobble alluvium we constructed reactor microcosms that imposed a diffusional gradient between sediment porewater and an overlying water column. Inside an anoxic glovebox 32 plastic (polypropylene) 3 cm tall tubes were packed with 8 g of oxbow lake sediment and then submerged in a 2 L reservoir of artificial groundwater (a sketch of the reactors is provided in SI Figure S3). This 2 L reservoir was referred to as the “advection solution”. Before packing, the sediment was homogenized and large organic debris (such as large roots) and pebbles were removed; however, no further attempts were made to select the particle size, and small roots were allowed to remain. Sediments were dominated by the smallest particle size fraction: 64% were between 53 and 150 μm in size and 22% were less than 53 μm in size (SI Table S3). The porosity of the sediment, measured by change in water content between saturation and oven-dry (24 h at 105 °C) was 0.48 ± 0.02 $cm^3\ g^{-1}$. The plastic tubes were sealed on all sides, except for the top (1.98 cm^2), ensuring that any mass exchanged must have occurred via diffusion across this interface.

A peristaltic pump supplied fresh artificial groundwater to the 2 L reservoir at a rate of 0.06 L $d^{-1}$for the first 8 days of the experiment and 0.12 L d^{-1} for the remainder of the

experiment. Solution was removed from the reservoir at the same flow rate, yielding a residence time of 33 days (first 8 days) to 17 days (remainder). The experiment was conducted for 85 days, which is comparable to the 3 week to 3 month duration of elevated water table excursions and oxidant concentrations observed in regional aquifers.(9) The composition of the artificial groundwater, which was based on the concentration of major cations and anions in groundwater at the Riverton site,(29) is given in the SI (Table S4). The pH of the influent groundwater solution was adjusted to 7.2. Three separate reactors were constructed, one in which the influent contained 1 mM NO_3^- (referred to as "Reactor-NO_3^-" or "R-NO_3^-"), one that was in equilibrium with air (yielding a dissolved O_2concentration of 250 μM; referred to as "Reactor-O_2" or "R-O_2"), and one that contained no oxidant (the artificial groundwater was anoxic; referred to as "Reactor-C" or "R-C"). The nitrate and control reactors were housed in a Coy anaerobic chamber with a H_2/N_2 atmosphere. The nitrate concentration was similar to groundwater concentrations measured at the Riverton site.(29) The oxygen reactor was stored on a benchtop in air. The influent reservoir that fed the 2 L reservoir of R-O_2 was constantly bubbled with air to ensure that the artificial groundwater was always saturated with O_2.

Measurement of Aqueous Ions in the Advection Solution

Aqueous samples were removed approximately daily from the 2 L reservoir of each of the three reactors, adjacent to the effluent outlet of the reactor. Five mL was preserved in 2% nitric acid (HNO_3) for analysis of U and Br via inductively coupled plasma-mass spectrometry (ICP-MS; Thermo XSeries II). Three mL was preserved frozen for analysis of NO_3^- and NO_2^- using colorimetry on a discrete analyzer (WestCo SmartChem 200). A volume of 1.5 mL was preserved in 0.1 M zinc chloride for analysis of S(-II). Sulfide was measured using the methylene blue colorimetric technique. Briefly, 60 μL each of 0.085 M N,N-dimethyl-1,4-phenylenediamine sulfate in 6 M HCl and 0.04 M ferric chloride in 6 M HCl were added to the preserved sample and allowed to react for at least 1 h. The light absorbed in the colored solutions was then measured at 600 nm using a UV–vis spectrometer (Shimadzu UV-1601).

Measurement of Ions in Sediment and Porewater

At select time points (days 2, 8, 22, 33, 57, 71, and 85), three sediment tubes were harvested from the reactor to monitor the concentration and oxidation state of U and other reactive species as a function of depth and time. The first tube was preserved frozen for μ-XAS analysis (either at −80 °C or in an anaerobic canister at −20 °C).

The second tube was sectioned into 0.5 cm segments. The porewater from these segments was extracted by centrifugation. An aliquot of the porewater (ca. 100 µL) was preserved frozen at −20 °C for measurement of aqueous NO_3^- and NO_2^- using a discrete analyzer. A second aliquot was diluted into 5 mL of 2% HNO_3 for measurement of U, Br and Fe via ICP-MS or inductively coupled plasma-optical emission spectrometry (ICP-OES; ThermoScientific ICAP 6300 Duo View Spectrometer). The remaining sediment was preserved in an anaerobic canister at −20 °C for bulk X-ray absorption spectroscopic analysis and for the measurement of sedimentary U concentration, which was determined via microwave digestion (due to limited mass of sediment) of ca. 0.1 g sediment in 10 mL concentrated HNO_3 for 2 h at 180 °C (in a CEM MarsExpress Microwave Digester). After digestion, the nitric acid was diluted in water and the U concentration was measured via ICP-MS. The total U concentration determined via digestion was 82% of that determined via XRF (based on comparison of the bulk, unreacted sediment measured via XRF and the sample from R-C, day 2, depth = 3 cm measured via digestion). Although digestion in HNO_3 did not recover 100% of the U determined via XRF, we expect the efficacy of the digestion to be comparable between days 2 and 85.

Fine-scale O_2 depth profiles were determined in a third tube by gold amalgam voltammetric microelectrodes(30) using a DLK-70 potentiostat equipped with automated micromanipulator (Analytical Instrument Systems, Inc. Flemington, NJ). The O_2 measurements were collected every 0.1 cm, starting 0.2 cm above the sediment-solution interface (reported as “-0.2 cm”) and proceeding 1.8 cm into the tube.

Bulk XAS

Uranium L_{III}-edge X-ray absorption spectra were collected at beamline 11–2 at the Stanford Synchtrotron Radiation Lightsource (SSRL). The energy of the X-ray beam was selected using a Si(220) φ = 0 double crystal monochromator detuned by 30% at 17,700 eV to minimize harmonics. Calibration was monitored during each sample scan by collecting the Y K-edge (17,038.4 eV). The fluorescence signal was monitored using a 100-element Ge detector. A strontium foil and Soller slits were used to increase the signal-to-noise ratio. Background normalization was performed in Athena(31) on spectra obtained from averaging 6–12 individual scans. No beam damage was observed between scans. To assess U oxidation state, linear combination fitting of the near-edge region was performed in Athena using a molecular U(IV) reference obtained from a pure

culture of U(VI) reducing bacteria(32) and U(VI) adsorbed to ferrihydrite. Shell-by-shell analysis of extended X-ray absorption fine edge structure (EXAFS) spectra was performed in Artemis with paths calculated (using FEFF 6 L(31)) based on the structures for uraninite,(33) rutherfordine,(34) and ningyoite(35) to obtain information on the local coordination environment of U (within 6 Å) (fitting details provided in SI).

Micro-XRF

Spatially resolved X-ray fluorescence spectromicroscopy was conducted to examine the distribution of U, Fe, S, Ca, Mn, and Ti in cross sections of the sediment tubes that were harvested on day 85. The preserved sediments were freeze-dried in their tubes, set in epoxy, and then cut in half (through their long axis) using a rock saw. The sectioned tubes were mounted at beamline 10–2 (SSRL). Maps were collected of the entire length of tube at 50 μm resolution at energies (selected using a Si(111) phi = 90 double crystal monochromator) above and below the U L_{III}-edge (17,200 eV and 17,000 eV), which enabled separation of the U fluorescence line from that of Rb, with which it overlaps. The fluorescent signal was detected using a single-element solid-state Vortex Si-drift detector. All data processing was conducted using the Microanalysis Toolkit software program.(36)

Results

Diffusivity of Sediments

The porewater concentration of the unreactive tracer bromide, Br^-, was measured to assess diffusion rates (Figure 1; also presented in this figure are the porewater concentrations of U, discussed below). We found that Br^- diffused into the sediment tubes rapidly compared to the time frame of the experiment. By day 2, porewater concentrations were 40–50% of the advection solution concentrations in all three reactors at the bottom of the sediment (3 cm). By day 8, the concentrations had reached 60% of the advection solution concentrations at the bottom of the sediment. By the end of the experiment (days 71 and 85), Br^- had completely diffused throughout the sediment profile; indeed its concentration in the porewater was higher than in the advection solution at some depths, which may indicate that Br^- did not behave in a completely conservative manner.

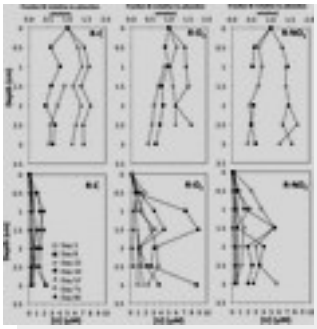

Figure 1. Depth profiles of aqueous Br and U porewater concentrations as a function of time. Note that the concentration at depth = 0 cm is the concentration of the analyte in the advection solution.

Efflux of Uranium from Sediments

Uranium concentrations in the advection solution reached their highest concentrations in all three reactors during the first 2 days of the experiment, and then decreased in concentration for the remainder of the experiment (Figure 2). The advection solution U concentration reached the highest levels in R-O_2, followed by R-NO_3^-. Although the concentration increased in R-C as well, the maximum was lower than in the reactors that contained oxidant; thus, we concluded that oxidation of sedimentary U caused its release into the advection solution in R-NO_3^- and R-O_2. The release of U from R-C sediments may have occurred due to U desorption or mobilization of U-containing colloids, which could have been facilitated when a small amount of sediment at the top of the tubes was suspended as the sediments were submerged in solution.

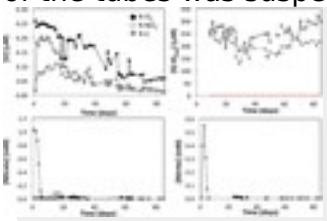

Figure 2. Aqueous U, S(-II), NO_3^-, and NO_2^- concentrations in advection solution versus time. The detection limit for [$S(-II)_{(aq)}$] (2 µM) is shown as a red line; all $S(-II)_{(aq)}$ concentrations in R-O_2 fell below the detection limit.

The net daily efflux of U from the sediments (J; µmol cm^{-2} d^{-1}) in all three reactors was estimated from the rate of change in the U concentration in the advection solution as a function of time, which was calculated based on the measured advection solution U concentration and the calculated loss of U in the reactor effluent (assuming that the concentration measured in the advection solution was equal to the concentration

leaving the reactor in the effluent; details of these calculations are provided in the SI; Figures S4 and S5). Net efflux of U from the sediments occurred only during the first 1–3 days of the experiment (for R-O_2, J = 0.0076 µmol cm^{-2} d^{-2}; for R-NO_3^-, J = 0.0031 µmol cm^{-2} d^{-2}; for R-C, J = 0.0015 µmol cm^{-2} d^{-2}); after which the flux of U was close to zero and the change in the advection solution U concentration was dominated by the removal of U in the effluent (SI Figure S4). The total percent of U released from the tubes relative to the total mass of U contained within the tubes was 0.13% (R-C), 0.33% (R-O_2) and 0.29% (R-NO_3^-). Thus, the majority of U was retained in the sediments, despite the continual supply of oxidant and the relatively rapid diffusion of solutes into the sediment tubes.

U in Porewaters and Sediments

Although the efflux of U from the sediments due to oxidation was only a small fraction of the total mass of U in the tubes, porewater concentrations of U in R-NO_3^- and R-O_2 were elevated relative to R-C, especially during the first 33 days of the experiment (Figure 1). For instance, the maximum U concentration in the porewater after 8 days was between ca. 6 and 9 µM for R-NO_3^- and R-O_2, whereas the concentration was only ca. 2 µM in the R-C porewater. Additionally, the porewater U concentration in the control reactor remained fairly constant over time; whereas the porewater U concentrations in R-NO_3^- and R-O_2 increased between days 2 and 8, and then decreased, finally reaching concentrations that were comparable to those observed in R-C by day 57.

The total amount of U released into the porewater was small relative to the amount of U stored within the sediment. For instance, the maximum porewater concentration was ca. 9 µM, which corresponds to only 0.2% of the total U contained in the sediment (including both the pore space and the solid phase). Analysis of the concentration of sedimentary U in the solid phase during day 2 and day 85 demonstrated that no significant sedimentary U loss occurred (SI Figure S6). Finally, analysis of U L_{III}-edge spectra of the sediments showed that sedimentary U(VI) did not accumulate between days 2 and 85 in any of the reactors (SI Figure S7 and Table S5). The top 0.5 cm of sediment contained U(VI) on day 2; however, this top layer contained only U(IV) during all subsequent measurements, indicating that any U(VI) initially generated migrated out of the sediments or was rereduced. Thus, it appears that the oxidants O_2 and NO_3^- caused a small amount of U to cycle between the sediments and the porewater, but did not result in either significant flux of U into the advection solution or the accumulation of U(VI) in the sediments.

Redox Poising of Sediments under the Different Treatment Conditions

Nondetectable levels of oxidant (O_2, NO_3^-, and NO_2^-) were observed in the R-C advection solution, nor was O_2 measured in R-C porewaters (Figures 2 and 3). Micromolar concentrations of NO_3^- (but not NO_2^-) were observed in R-C porewaters on day 2, but these could reflect native porewater concentrations of NO_3^-, as they were within the range observed in Riverton groundwater.(29) Additionally, several hundred micromolar S(-II) was observed in the advection solution. The absence of oxidants and production of aqueous S(-II) indicates that R-C sediments (and advection solution) were reducing.

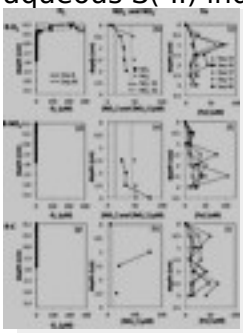

Figure 3. Aqueous NO_3^-, NO_2^-, Fe, and O_2 in porewater versus depth. The concentration of aqueous redox-active species as a function of depth is presented for each of the reactors. The concentration of the N species is only provided for day 2. The detection limit for the N species was relatively high and is shown on the plots ("DL"); NO_3^- and NO_2^- concentrations were not plotted if they fell below the detection limit. Note that the concentration at depth = 0 cm is the concentration of the analyte (Fe, $NO_3^-$and NO_2^-) in the advection solution and that the concentration of NO_3^- and NO_2^- are not plotted at 0 cm for R-NO_3^- to enhance visualization of the porewater concentrations.

Oxygen was consumed rapidly within R-O_2 sediments: its concentration decreased below detection within the first 0.25 cm at the beginning of the experiment (8 days) and at the end (85 days) (Figure 3). Both NO_3^- and NO_2^- were detected in R-O_2 porewaters, suggesting that N cycling was induced in the sediments (Figure 3). Porewater Fe was elevated in R-O_2 sediments, particularly at a depth of 1 cm (Figure 3). Divalent Fe is much more soluble than Fe(III),(37) thus we infer that the porewater Fe concentrations, which ranged from ca. 10–100 μM were indicative of soluble Fe(II) production. Although elevated Fe concentrations could also indicate that trivalent Fe colloids formed, we note that (1) Fe concentrations were also elevated in R-C and (2) porewater Fe concentrations peaked in R-O_2 sediments just below the depth at which O_2 was depleted, suggesting Fe(III) reduction led to high aqueous Fe. Sulfide was never detected

(detection limit = 0.3 μM) in the advection solution of RO_2, indicating that S(-II) generated in the sediments was oxidized before reaching the advection solution. Even though the R-NO_3^- influent contained 1 mM NO_3^-, its concentration in the advection solution decreased below detection within the first week and remained below detection for the rest of the 85-day experiment (Figure 2), suggesting rapid denitrification. Nitrite was produced during the first week in the advection solution, increasing to 0.55 mM and then decreasing below detection for the remainder of the experiment (Figure 2). Relatively little NO_3^- was detected in RNO_3^- porewaters (day 2) (Figure 3). Indeed the concentration of NO_3^- in R-NO_3^- was similar to the concentrations observed in R-C and R-O_2. However, micromolar concentrations of porewater NO_2^- were observed, indicating denitrification occurred within the sediments, as well in the advection solution. Concomitant with removal of NO_3^-, several hundred micromolar $S(-II)_{(aq)}$ was observed in the advection solution (Figure 2), indicating the onset of reducing conditions.

Speciation and Microscale Distribution of Sedimentary U(IV)

Under all treatment conditions, U was located throughout the entire sediment profile on day 85 and was distributed in hot spots ranging from tens of microns to approximately millimeters in size (Figure 4). The U distribution was not highly correlated with the distributions of Fe, Mn, Ti, S or Ca at 50 μm resolution: the highest U intensities were observed where the intensities of other elements were relatively low; whereas the highest intensities of other elements were observed where U intensities were low (Figures S8 - S10).

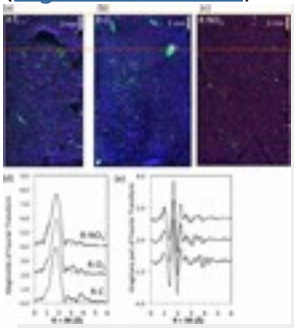

Figure 4. Sedimentary U speciation and distribution (day 85). X-ray fluorescent maps for cross sections of sediment tubes harvested on day 85 are shown in (a)–(c). The U distribution is shown in green, Fe in red and S in blue. The intensity values of the S and Fe pixels were scaled to 25% of the S and Fe maximum intensity to enhance contrast. The intensity values of the U pixels were scaled to 50% of the U maximum intensity. The magnitude and imaginary parts of the Fourier transformed EXAFS spectra for the top 0.5 cm of the sediment tubes (indicated by

the orange box) are shown in (d) and (e), respectively. Data is shown in black, fits are shown in gray.

Fourier transformed EXAFS spectra (Figure 4) that were collected from the 0–0.5 cm fraction of each sediment tube (RO_2, RNO_3^-, and RC) on day 85 did not exhibit a prominent peak at ca. 3.6 Å (R + δR), which is characteristic of UO_2 formation.(38, 39) Attempts to fit small peaks at *ca*. 3.6 Å yielded coordination numbers close to 1 with errors ≥100% (even when Debye–Waller factors were constrained based on literature values for biogenic UO_2(40)), suggesting that very little $UO_2$was present. Instead, we employed a model in which U(IV) was bound to organic carbon, consistent with previous research indicating U has a high affinity for organic matter.(38, 40-43) Our model comprised U(IV) bound to oxygen ligands in a first shell at 2.31–2.34 Å, followed by 2–4 C ligands in a second shell at 2.85–2.86 Å (Figure 4 and SI Table S6). The fitted bond distances were consistent with those reported previously for similar models.(38, 40) The number of coordinating oxygen atoms was higher than is typical for U, suggesting that there was a large amount of structural disorder in the U–O bond distance.(38) However, attempts to replace or augment the U–C shell with a second U–O shell yielded physically unrealistic fitting parameters, despite constraints placed on the U–O coordination numbers and Debye–Waller factors. Fits with P backscatterers also yielded physically unreasonable fits. Thus, we infer that U(IV) was likely bound to carbon ligands; however, regardless of the identity of the second shell neighbor, our EXAFS analysis demonstrated that UO_2 was a minor species. Finally, we note that UO_2 was not present in unaltered sediment (i.e., sediment that was not exposed to reactor conditions), either (see SI, Figure S11 and Table S6). We also note that we did not collect EXAFS spectra for sediments on day 2 of the experiment, and are thus unable to observe whether changes in U speciation occurred between day 0 and day 2, although we expect that uraninite would not have been dominant on day 2, since it was not dominant on day 0 or on day 85.

Discussion

The higher porewater and advection solution U concentrations in R-O_2 and R-NO_3^- relative to R-C suggest O_2 and NO_3^- caused U oxidation, which may have occurred directly or via reaction with products generated from O_2 and NO_3^- consumption, such as

NO_2^-, NO, N_2O, and Fe(III). The maximum efflux occurred (day 1) before the maximum porewater concentrations occurred (day 8), which indicates that the initial pulse of U to the advection solution likely came from oxidation in the very upper layer of sediment. It is unlikely that U located deeper within the sediment was released into the advection solution, otherwise continued release of U into the advection solution would have been observed while porewater concentrations were elevated between days 2 and 33. This implies that some mechanism existed whereby porewater U was reincorporated into the sediments, such as reduction of U(VI) and adsorption of U(IV) (see Discussion below).

We expected that the greatest porewater U concentrations would be observed close to the sediment-advection solution interface where oxidant concentrations were highest; however, the concentration of U in the first 0.5 cm of the sediment was typically lower than the U concentration in the porewater from the lower depths (1–1.5 cm). This pattern may suggest that reactive intermediates (e.g., Fe(III), NO, N_2O, and NO_2^-) built up at these intermediate depths because the reactions responsible for their generation were not at steady state. Evidence for this assertion comes from inspection of the depth profiles of porewater NO_2^- in R-NO_3^-. Nitrite was only detectable below the 0–0.5 cm depth, suggesting it was removed too rapidly to generate U(VI) at the top of the sediment. In R-O_2 porewater Fe concentrations peaked at a depth of 1 cm, which we interpreted to arise from Fe(III) reduction. Cycling of even a small percentage of this Fe(II) back to Fe(III) (caused, for instance, by reaction with NO_2^- or the coupling of Fe(II) oxidation to nitrate reduction(13, 23)) could yield reactive Fe(III) species that then oxidized U(IV).(23)

One other explanation for porewater release of U in R-O_2 and R-NO_3 must be considered: U(IV) may have been mobilized in association with colloids released due to changing geochemical conditions within the sediments induced by O_2 or NO_3^-. Uranium(IV)-containing colloids have been observed in groundwater and wetlands.(44) Furthermore, iron-reducing conditions can result in the release of colloids due to an increase in pH above the point of zero charge(45) or the dissolution of Fe(III) oxides that are aggregated with organic matter (leading to release of Fe(II) in conjunction with organic colloids).(46) Colloidal release of U(IV) could be particularly relevant at depths at or below 1 cm in R-O_2, where we have proposed that Fe(III) reduction led to the large observed increase in the porewater Fe concentration. Dissolution of Fe(III) aggregated with organic-bound U(IV) could have yielded elevated U porewater concentrations.

However, sulfides are well-known to reduce Fe(III) oxides, yet SO_4^{2-} reduction and elevated porewater Fe concentrations in R-C were not associated with elevated porewater U concentrations.

Regardless of the mechanism of U release into sediment porewaters, by day 57 U concentrations in R-O_2 and R-NO_3^- decreased to the levels observed in R-C, despite the fact that oxidant was supplied via the influent throughout the 85-day experimental period, indicating that processes attenuating aqueous U concentrations or inhibiting U(IV) oxidation eventually dominated the geochemistry of the system.

Although transport properties likely impacted the development of redox conditions in the sediments (discussed above), the rapid influx of Br^- into the sediment tubes suggested that the entire length of tube should have been exposed to oxidant during the course of the experiment were oxidants transported conservatively. Thus, although, previous work suggests that oxidation of U(IV) occurs more slowly in the field than in the laboratory under completely mixed conditions,(47)we infer that diffusion-limited flow could not, in itself, have inhibited U release to the overlying advection solution.

Many researchers have focused on the kinetic limitations of U(IV) oxidation, as U(VI) can be resistant to oxidation if it exists as large crystals on UO_2(20) or if nanoparticles of UO_2 become passivated by Ca^{2+} or Mg^{2+} adsorption.(17) In contrast, oxidation of noncrystalline U(IV) species produced by bacteria occurs rapidly (over the course of a few hours) under aerated, well-mixed conditions in the laboratory.(20) EXAFS spectroscopic analysis of U(IV) speciation in our experimental sediments revealed that U(IV) did not occur predominantly as UO_2 (either at the beginning or end of the experiment) and may have been bound to C in a second shell. Furthermore, U was found in large hot spots that did not coincide with hot spots of elements that comprise major sedimentary minerals (Fe, Mn, Ti, S, and Ca). In a peat soil, Mikutta et al. (38)observed similar U hot spots, which they argued represented U associated with particulate organic carbon, leading us to posit that U was associated with organic carbon in our sediments, as well (μ-XRF cannot detect C). This interpretation is consistent with previous research showing U(IV) exhibits high affinities for organic functional groups(40-42) and will bind to organics in sediments.(38, 43) We expect that organic-bound U(IV) in the reactor sediments was not resistant to oxidation, as has been observed previously in laboratory systems,(20) which would suggest that the rate of U(IV) oxidation was not the major limitation on the amount of U released from the

sediments. Although we cannot rule out the possibility that the organic-U(IV) complexes in the reactor sediments were more resistant to oxidation than those examined in laboratory studies, the kinetic-lability of the sedimentary U(IV) is consistent with our observation that the elevated advection solution and porewater U concentrations occurred during early time points (1–33 days) and decreased with longer exposure to O_2 and NO_3^-.

Researchers have posited that reduced species, such as Fe(II) and S(-II), can prevent U(IV) oxidation by attenuating oxidant concentrations.(9, 21, 22, 48) However, our results suggest that consumption of oxidant by inorganic reductants was not the major limitation on U(VI) mobilization, as Fe(II) and S(-II) were produced, not consumed, during the experiment. Instead, we propose that the dominant factor preventing U(IV) oxidation and subsequent mobilization from the sediments into the advection solution was the availability of organic matter in the sediments to fuel rapid microbial respiration, causing O_2 and NO_3^- to be consumed close to the sediment-advection solution interface and Fe(III) and SO_4^{2-} to be consumed at depth. Because U mobilization decreased with continued exposure to O_2 and NO_3^-, it is interesting to speculate whether oxidant intrusion into the sediments could in fact contribute to U *immobilization* over time by increasing the microbial availability of organic carbon. Oxygen is well-known to enhance production of low molecular weight organic compounds that stimulate metal- and sulfate-reducing bacteria;(49)furthermore, Fe(III)-reducing bacteria could further enhance organic matter mineralization through dissolution of Fe(III)–organic matter aggregates.(50)

Environmental Implications

Although studies have focused on kinetic controls on U(IV) oxidation,(20) as well as buffering of U(IV) oxidation by inorganic reductants,(9) we suggest that the primary criterion for assessing whether sedimentary U(IV) will be mobile in the field should be the sediment's ability to resist changes to its redox potential upon exposure to oxidizing conditions, particularly imparted by its organic matter content. This is relevant as studies of U-contaminated aquifers show that reduced sediments vary in their response to redox perturbations as a result of differences in sediment texture (which impart diffusional limitations),(18) proximity to the water table(18) and organic matter content and quality.(27) Indeed, Lezama et al.(17) observed that oxidative U mobilization varied between two sediment wells with different redox characteristics(3) within the same

aquifer over the course of seasonal water table excursions. The O_2 concentration spiked to much higher levels in one well than in the other, resulting in either full or insignificant U release.(17) This implies that it will be important to employ models of U oxidation that incorporate information on aquifer sediment heterogeneities, which yield differences in microbial respiration rates, as has been done recently for organic carbon mineralization.(28) We note here the importance of heterogeneities in sediment texture, which impart diffusional limitations that in turn impose gradients in electron acceptors, electron donors and other redox active species, as we observed in the reactor porewaters. Finally, our results demonstrate that, for sediments with fine textures and ample organic carbon, seasonal influxes of O_2 and NO_3^- may cause only localized mobilization of U without leading to export of U from the reducing sediments.

Supporting Information

The Supporting Information is available free of charge on the ACS Publications website at DOI: 10.1021/acs.est.7b02241.

- Spectroscopic characterization of Fe and S speciation in the sediment, reactor design, particle size, artificial groundwater composition, flux calculations, sedimentary U content and oxidation state, correlation between U and elements measured via μ-XRF, fitting parameters for EXAFS spectroscopic analysis (PDF)

- **PDF**
  - es7b02241_si_002.pdf (1.42 MB)

Oxidative Uranium Release from Anoxic Sediments under Diffusion-Limited Conditions

S1

Oxidative uranium release from anoxic sediments under diffusion-limited conditions

Supporting Information

Sharon E. Bone[1*†], Melanie R. Cahill[2], Morris

E. Jones[2§], Scott Fendorf[2], James Davis[3], Kenneth H. Williams[4], John R. Bargar[1*]

*Corresponding Author, shbone@lanl.gov

[1]Stanford Synchrotron Radiation Laboratory, SLAC National Accelerator Laboratory, Menlo Park, CA 94025

[2]Stanford University, Stanford, CA 94305

[3]US Geological Survey, Menlo Park, CA 94025

[4]Lawrence Berkeley National Laboratory, Berkeley, CA 94720

†Present address: Los Alamos National Laboratory, Los Alamos, NM 87545

§Present address: University of Massachusetts Amherst, Amherst, MA 01003

22 pages

6 Tables

11 Figures

S2

The S speciation of the sediments was examined using K-edge X-ray absorption near edge structure (XANES) spectroscopy, which was performed at the Stanford Synchrotron Radiation Light source (SSRL). Samples were prepared for S XANES spectroscopy by drying an aliquot of the sediment that was not exposed to the react

or conditions, grinding in a mortar and pestle, and depositing < 10 mg on a piece of low-S Mylar tape. The S K-edge was collected at beamline 4-3 in fluorescence mode using a silicon drift detector. The samples were contained in a sample chamber filled with helium during the measurements, which were performed at room temperature. Calibration was performed approximately every eight hours using a sodium thiosulfate standard (2472.02 eV). The identity of different S oxidation states was determined by linear combination fitting using reference S compounds. The Fe speciation of the sediments was examined using K-edge XANES spectroscopy in a sample that was harvested from the 2.5–3 cm depth of the control reactor on day 2. Sediments were stored frozen before analysis and were thawed and then mounted into slotted aluminum sample holders and sealed with Katpon tape immediately before placing in the sample chamber at the beamline. The sample chamber was evacuated to 10^{-6} torr, providing an anoxic environment for the samples during the measurements. The Fe K-edge was collected at SSRL beamline 4-1 in fluorescence mode using a passivated implanted planar silicon (PIPS) detector. Measurements were made at 77 K in a liquid nitroge

n cryostat. The monochromator crystals were detuned 40 % at 7,600 eV to minimize harmonics. A

figshare

Share**Download**

⊥Author Present Address

(S.E.B.) Los Alamos National Laboratory, Los Alamos, Nnew Mexico 87545, United States

#Author Present Address

(M.E.J.) University of Massachusetts Amherst, Amherst, Massachusetts 01003, United States

The authors declare no competing financial interest.

Acknowledgment

Funding for S.E.B. was provided by the DOE Office of Biological and Environmental Research, Subsurface Biogeochemistry Research (SBR) activity to the SLAC SFA program under contract DE-AC02-76SF00515 to SLAC and by Lawrence Berkeley National Laboratory (DE-AC02-05CH11231) with funding from the U.S. Department of Energy (DOE), Office of Legacy Management. Use of SSRL is supported by the U.S. DOE, Office of Basic Energy Sciences under Contract No. DE-AC02-76SF00515.

Reference QuickView

References

This article references 50 other publications.

1. 1.

Abdelouas, A. Uranium mill tailings: geochemistry, mineralogy, and environmental impact *Elements* **2006**, 2,335– 341 DOI: 10.2113/gselements.2.6.335

[Crossref], [CAS]

2. 2.

Williams, K. H.; Bargar, J. R.; Lloyd, J. R.; Lovley, D. R. Bioremediation of uranium-contaminated groundwater: a systems approach to subsurface biogeochemistry *Curr. Opin. Biotechnol.* **2013**, 24 (3) 489–497 DOI: 10.1016/j.copbio.2012.10.008

[Crossref], [PubMed], [CAS]

3. 3.

Campbell, K. M.; Kukkadapu, R. K.; Qafoku, N. P.; Peacock, A. D.; Lesher, E.; Williams, K. H.; Bargar, J. R.;Wilkins, M. J.; Figueroa, L.; Ranville, J.; Davis, J. A.; Long, P. E. Geochemical, mineralogical and microbiological characteristics of sediment from a naturally reduced zone in a uranium-contaminated aquifer*Appl. Geochem.* **2012**, 27 (8) 1499– 1511 DOI: 10.1016/j.apgeochem.2012.04.013

[Crossref], [CAS]

4. 4.

Janot, N.; Pacheco, J. S. L.; Pham, D. Q.; O'Brien, T. M.; Hausladen, D.; Noel, V.; Lallier, F.; Maher, K.;Fendorf, S.; Williams, K. H.; Long, P. E.; Bargar, J. R. Physico-Chemical Heterogeneity of Organic-Rich Sediments in the Rifle Aquifer, CO: Impact on Uranium Biogeochemistry *Environ. Sci. Technol.* **2016**, 50 (1)46– 53 DOI: 10.1021/acs.est.5b03208

[ACS Full Text], [CAS]

5. 5.

Maher, K.; Bargar, J. R.; Brown, G. E., Jr. Environmental speciation of actinides *Inorg. Chem.* **2013**, 52 (7)3510– 3532 DOI: 10.1021/ic301686d

[ACS Full Text], [CAS]

6. 6.

Williams, K. H.; Long, P. E.; Davis, J. A.; Wilkins, M. J.; N'Guessan, A. L.; Steefel, C. I.; Yang, L.;Newcomer, D.; Spane, F. A.; Kerkhof, L. J.; McGuinness, L.; Dayvault, R.; Lovley, D. R. Acetate availability and its influence on sustainable bioremediation of uranium-contaminated groundwater *Geomicrobiol. J.***2011**, 28 (5–6) 519– 539 DOI: 10.1080/01490451.2010.520074

[Crossref], [CAS]

7. 7.

Dam, W. L.; Campbell, S.; Johnson, R. H.; Looney, B. B.; Denham, M. E.; Eddy-Dilek, C. A.; Babits, S. J.Refining the site conceptual model at a former uranium mill

site in Riverton, Wyoming, USA *Environ. Earth Sci.* **2015**, 74 (10) 7255– 7265 DOI: 10.1007/s12665-015-4706-y

[Crossref]

8. 8.

Zachara, J. M.; Long, P. E.; Bargar, J.; Davis, J. A.; Fox, P.; Fredrickson, J. K.; Freshley, M. D.;Konopka, A. E.; Liu, C. X.; McKinley, J. P.; Rockhold, M. L.; Williams, K. H.; Yabusaki, S. B. Persistence of uranium groundwater plumes: Contrasting mechanisms at two DOE sites in the groundwater-river interaction zone *J. Contam. Hydrol.* **2013**, 147, 45– 72 DOI: 10.1016/j.jconhyd.2013.02.001

[Crossref], [PubMed], [CAS]

9. 9.

Yabusaki, S. B.; Wilkins, M. J.; Fang, Y. L.; Williams, K. H.; Arora, B.; Bargar, J.; Beller, H. R.; Bouskill, N. J.;Brodie, E. L.; Christensen, J. N.; Conrad, M. E.; Danczak, R. E.; King, E.; Soltanian, M. R.; Spycher, N. F.;Steefel, C. I.; Tokunaga, T. K.; Versteeg, R.; Waichler, S. R.; Wainwright, H. M. Water Table Dynamics and Biogeochemical Cycling in a Shallow, Variably-Saturated Floodplain *Environ. Sci. Technol.* **2017**, 51 (6)3307– 3317 DOI: 10.1021/acs.est.6b04873

[ACS Full Text], [CAS]

10. 10.

Hill, A. R. Buried organic-rich horizons: their role as nitrogen sources in stream riparian zones*Biogeochemistry* **2011**, 104 (1–3) 347– 363 DOI: 10.1007/s10533-010-9507-5

[Crossref], [CAS]

11. 11.

Senko, J. M.; Istok, J. D.; Suflita, J. M.; Krumholz, L. R. In-situ evidence for uranium immobilization and remobilization *Environ. Sci. Technol.* **2002**, 36 (7) 1491– 1496 DOI: 10.1021/es011240x

[ACS Full Text], [CAS]

12. 12.

Beller, H. R. Anaerobic, nitrate-dependent oxidation of U(IV) oxide minerals by the chemolithoautotrophic bacterium *Thiobacillus denitrificans Appl. Environ. Microbiol.* **2005**, 71 (4) 2170– 2174 DOI: 10.1128/AEM.71.4.2170-2174.2005

[Crossref], [PubMed], [CAS]

13. 13.

Senko, J. M.; Suflita, J. M.; Krumholz, L. R. Geochemical controls on microbial nitrate-dependent U(IV) oxidation *Geomicrobiol. J.* **2005**, 22 (7–8) 371– 378 DOI: 10.1080/01490450500248911

[Crossref], [CAS]

14. 14.

Finneran, K. T.; Housewright, M. E.; Lovley, D. R. Multiple influences of nitrate on uranium solubility during bioremediation of uranium-contaminated subsurface sediments *Environ. Microbiol.* **2002**, 4 (9) 510– 516DOI: 10.1046/j.1462-2920.2002.00317.x

[Crossref], [PubMed], [CAS]

15. 15.

Wu, W. M.; Carley, J.; Green, S. J.; Luo, J.; Kelly, S. D.; Van Nostrand, J.; Lowe, K.; Mehlhorn, T.;Carroll, S.; Boonchayanant, B.; Lofller, F. E.; Watson, D.; Kemner, K. M.; Zhou, J. Z.; Kitanidis, P. K.;Kostka, J. E.; Jardine, P. M.; Criddle, C. S. Effects of nitrate on the stability of uranium in a bioreduced region of the subsurface *Environ. Sci. Technol.* **2010**, 44 (13) 5104– 5111 DOI: 10.1021/es1000837

[ACS Full Text], [CAS]

16. 16.

Istok, J. D.; Senko, J. M.; Krumholz, L. R.; Watson, D.; Bogle, M. A.; Peacock, A.; Chang, Y. J.; White, D. C.In situ bioreduction of technetium and uranium in a nitrate-contaminated aquifer *Environ. Sci. Technol.* **2004**,38 (2) 468– 475 DOI: 10.1021/es034639p

[ACS Full Text], [CAS]

17. 17.

Lezama-Pacheco, J. S.; Cerrato, J. M.; Veeramani, H.; Alessi, D. S.; Suvorova, E.; Bernier-Latmani, R.;Giammar, D. E.; Long, P. E.; Williams, K. H.; Bargar, J. R. Long-Term in Situ Oxidation of Biogenic Uraninite in an Alluvial Aquifer: Impact of Dissolved Oxygen and Calcium *Environ. Sci. Technol.* **2015**, 49 (12) 7340–7347 DOI: 10.1021/acs.est.5b00949

[ACS Full Text], [CAS]

18. 18.

Noel, V.; Boye, K.; Kakkadapu, R. K.; Bone, S. E.; Pacheco, J. S. L.; Cardarelli, E.; Janot, N.; Fendorf, S.;Williams, K. H.; Bargar, J. R. Understanding

controls on redox processes in floodplain sediments of the Upper Colorado River Basin *Sci. Total Environ.* **2017**, 603, 663– 675 DOI: 10.1016/j.scitotenv.2017.01.109

[Crossref], [PubMed], [CAS]

19. 19.

Ulrich, K.-U.; Ilton, E. S.; Veeramani, H.; Sharp, J. O.; Bernier-Latmani, R.; Schofield, E. J.; Bargar, J. R.;Giammar, D. E. Comparative dissolution kinetics of biogenic and chemogenic uraninite under oxidizing conditions in the presence of carbonate *Geochim. Cosmochim. Acta* **2009**, 73 (20) 6065– 6083 DOI: 10.1016/j.gca.2009.07.012

[Crossref], [CAS]

20. 20.

Cerrato, J. M.; Ashner, M. N.; Alessi, D. S.; Lezama-Pacheco, J. S.; Bernier-Latmani, R.; Bargar, J. R.;Giammar, D. E. Relative reactivity of biogenic and chemogenic uraninite and biogenic noncrystalline U(IV)*Environ. Sci. Technol.* **2013**, 47 (17) 9756– 9763 DOI: 10.1021/es401663t

[ACS Full Text], [CAS]

21. 21.

Carpenter, J.; Bi, Y. Q.; Hayes, K. F. Influence of Iron Sulfides on Abiotic Oxidation of UO2 by Nitrite and Dissolved Oxygen in Natural Sediments *Environ. Sci. Technol.* **2015**, 49 (2) 1078– 1085 DOI: 10.1021/es504481n

[ACS Full Text], [CAS]

22. 22.

Paradis, C. J.; Jagadamma, S.; Watson, D. B.; McKay, L. D.; Hazen, T. C.; Park, M.; Istok, J. D. In situ mobility of uranium in the presence of nitrate following sulfate-reducing conditions *J. Contam. Hydrol.* **2016**,187, 55– 64 DOI: 10.1016/j.jconhyd.2016.02.002

[Crossref], [PubMed], [CAS]

23. 23.

Senko, J. M.; Mohamed, Y.; Dewers, T. A.; Krumholz, L. R. Role for Fe(III) minerals in nitrate-dependent microbial U(IV) oxidation *Environ. Sci. Technol.* **2005**, 39 (8) 2529– 2536 DOI: 10.1021/es048906i

[ACS Full Text], [CAS]

24. 24.

N’Guessan, A. L.; Moon, H. S.; Peacock, A. D.; Tan, H.; Sinha, M.; Long, P. E.; Jaffe, P. R.Postbiostimulation microbial community structure changes that control the reoxidation of uranium *FEMS Microbiol. Ecol.* **2010**, 74 (1) 184– 195 DOI: 10.1111/j.1574-6941.2010.00933.x

[Crossref], [PubMed], [CAS]

25. 25.

LaRowe, D. E.; Van Cappellen, P. Degradation of natural organic matter: a thermodynamic analysis*Geochim. Cosmochim. Acta* **2011**, 75 (8) 2030– 2042 DOI: 10.1016/j.gca.2011.01.020

[Crossref], [CAS]

26. 26.

Jin, Q.; Bethke, C. M. Predicting the rate of microbial respiration in geochemical environments *Geochim. Cosmochim. Acta* **2005**, 69 (5) 1133– 1143 DOI: 10.1016/j.gca.2004.08.010

[Crossref], [CAS]

27. 27.

Boye, K.; Noel, V.; Tfaily, M. M.; Bone, S. E.; Williams, K. H.; Bargar, J. R.; Fendorf, S. Thermodynamically controlled preservation of organic carbon in floodplains *Nat. Geosci.* **2017**, 10 (6) 415– 419 DOI: 10.1038/ngeo2940

[Crossref], [CAS]

28. 28.

Arora, B.; Spycher, N. F.; Steefel, C. I.; Molins, S.; Bill, M.; Conrad, M. E.; Dong, W. M.; Faybishenko, B.;Tokunaga, T. K.; Wan, J. M.; Williams, K. H.; Yabusaki, S. B. Influence of hydrological, biogeochemical and temperature transients on subsurface carbon fluxes in a flood plain environment *Biogeochemistry* **2016**, 127(2–3) 367– 396 DOI: 10.1007/s10533-016-0186-8

[Crossref], [CAS]

29. 29.

U.S. Department of Energy. Legacy Management Geospatial Environmental Mapping System.http://gems.lm.doe.gov/imf/ext/gems/jsp/launch.jsp.

30. 30.

Brendel, P. J.; Luther, G. W. Development of a gold amalgam voltammetric microelectrode for the determination of dissolved Fe, Mn, O2, and S(-II) in

porewaters of marine and fresh-water sediments*Environ. Sci. Technol.* **1995**, 29 (3) 751– 761 DOI: 10.1021/es00003a024

[ACS Full Text], [CAS]

31. 31.

Ravel, B.; Newville, M. Athena, Artemis, Hephaestus: data analysis for X-ray absorption spectroscopy using IFFEFIT *J. Synchrotron Radiat.* **2005**, 12, 537– 541 DOI: 10.1107/S0909049505012719

[Crossref], [PubMed], [CAS]

32. 32.

Alessi, D. S.; Uster, B.; Borca, C. N.; Grolimund, D.; Bernier-Latmani, R. Beam-induced oxidation of monomeric U(IV) species *J. Synchrotron Radiat.* **2013**, 20 (1) 197– 199 DOI: 10.1107/S0909049512041763

[Crossref], [PubMed], [CAS]

33. 33.

Wyckoff, R. W. G. *Crystal Structures 1*, 2nd ed.; Interscience Publishers: New York, NY, **1963**.

34. 34.

Finch, R.; Cooper, M. A.; Hawthorne, F. C.; Ewing, R. C. Refinement of the crystal structure of rutherfordine*Canadian Mineralogist* **1999**, 37, 929– 938

[CAS]

35. 35.

Anthony, J. W.; Bideaux, R. A.; Bladh, K. W.; Nichols, M. C. *Handbook of Mineralogy*. Mineralogical Society of America: Chantilly, VA.

36. 36.

Webb, S. M. Microanalysis Toolkit software program, v1.40; Stanford Synchrotron Radiation Lightsource,**2006**.

37. 37.

Rickard, D.; Luther, G. W. Chemistry of iron sulfides *Chem. Rev.* **2007**, 107 (2) 514– 562 DOI: 10.1021/cr0503658

[ACS Full Text], [CAS]

38. 38.

Mikutta, C.; Langner, P.; Bargar, J. R.; Kretzschmar, R. Tetra- and Hexavalent Uranium Forms Bidentate-Mononuclear Complexes with Particulate Organic Matter in a Naturally Uranium-Enriched Peatland *Environ. Sci. Technol.* **2016**, 50 (19) 10465– 10475 DOI: 10.1021/acs.est.6b03688

[ACS Full Text], [CAS]

39. 39.

Alessi, D. S.; Uster, B.; Veeramani, H.; Suvorova, E. I.; Lezama-Pacheco, J. S.; Stubbs, J. E.; Bargar, J. R.;Bernier-Latmani, R. Quantitative Separation of Monomeric U(IV) from UO2 in Products of U(VI) Reduction*Environ. Sci. Technol.* **2012**, 46 (11) 6150– 6157 DOI: 10.1021/es204123z

[ACS Full Text], [CAS]

40. 40.

Boyanov, M. I.; Fletcher, K. E.; Kwon, M. J.; Rui, X.; O'Loughlin, E. J.; Loffler, F. E.; Kemner, K. M. Solution and microbial controls on the formation of reduced U(IV) species *Environ. Sci. Technol.* **2011**, 45 (19) 8336–8344 DOI: 10.1021/es2014049

[ACS Full Text], [CAS]

41. 41.

Alessi, D. S.; Lezama-Pacheco, J. S.; Stubbs, J. E.; Janousch, M.; Bargar, J. R.; Persson, P.;Bernier-Latmani, R. The product of microbial uranium reduction includes multiple species with U(IV)-phosphate coordination *Geochim. Cosmochim. Acta* **2014**, 131, 115– 127 DOI: 10.1016/j.gca.2014.01.005

[Crossref], [CAS]

42. 42.

Stylo, M.; Alessi, D. S.; Shao, P. P.; Lezama-Pacheco, J. S.; Bargar, J. R.; Bernier-Latmani, R.Biogeochemical Controls on the Product of Microbial U(VI) Reduction *Environ. Sci. Technol.* **2013**, 47 (21)12351– 12358 DOI: 10.1021/es402631w

[ACS Full Text], [CAS]

43. 43.

Bone, S. E.; Dynes, J. J.; Cliff, J.; Bargar, J. R. Uranium(IV) adsorption by natural organic matter in anoxic sediments *Proc. Natl. Acad. Sci. U. S. A.* **2017**, 114 (4) 711– 716 DOI: 10.1073/pnas.1611918114

[Crossref], [PubMed], [CAS]

44. 44.

Wang, Y.; Frutschi, M.; Suvorova, E.; Phrommavanh, V.; Descostes, M.; Osman, A. A. A.; Geipel, G.;Bernier-Latmani, R. *Nat. Commun.* **2013**, 4, 2942– 2951 DOI: 10.1038/ncomms3942

[Crossref], [PubMed], [CAS]

45. 45.

Thompson, A.; Chadwick, O. A.; Boman, S.; Chorover, J. Colloid mobilization during soil iron redox oscillations *Environ. Sci. Technol.* **2006**, 40 (18) 5743– 5749 DOI: 10.1021/es061203b

[ACS Full Text], [CAS]

46. 46.

Buettner, S. W.; Kramer, M. G.; Chadwick, O. A.; Thompson, A. Mobilization of colloidal carbon during iron reduction in basaltic soils *Geoderma* **2014**, 221–222, 139– 145 DOI: 10.1016/j.geoderma.2014.01.012

[Crossref], [CAS]

47. 47.

Campbell, K. M.; Veeramani, H.; Ulrich, K. U.; Blue, L. Y.; Giammar, D. E.; Bernier-Latmani, R.;Stubbs, J. E.; Suvorova, E. I.; Yabusaki, S. B.; Lezama-Pacheco, J. S.; Mehta, A.; Long, P. E.; Bargar, J. R.Oxidative dissolution of biogenic uraninite in gorundwater at Old Rifle, Co *Environ. Sci. Technol.* **2011**, 45,8748– 8754 DOI: 10.1021/es200482f

[ACS Full Text], [CAS]

48. 48.

Bi, Y.; Hayes, K. F. Surface Passivation Limited UO2 Oxidative Dissolution in the Presence of FeS *Environ. Sci. Technol.* **2014**, 48 (22) 13402– 13411 DOI: 10.1021/es5041392

[ACS Full Text], [CAS]

49. 49.

Keiluweit, M.; Nico, P. S.; Kleber, M.; Fendorf, S. Are oxygen limitations under recognized regulators of organic carbon turnover in upland soils? *Biogeochemistry* **2016**, 127 (2–3) 157– 171 DOI: 10.1007/s10533-015-0180-6

[Crossref], [CAS]

50. 50.

Keiluweit, M.; Bougoure, J. J.; Nico, P. S.; Pett-Ridge, J.; Weber, P. K.; Kleber, M. Mineral protection of soil carbon counteracted by root exudates *Nat. Clim. Change* **2015**, 5 (6) 588– 595 DOI: 10.1038/nclimate2580

[Crossref], [CAS]